Bending Tests for the Structural Safety Assessment of Space Truss Members

Marco Bonopera[1,3*], Kuo-Chun Chang[2], Chun-Chung Chen[3], Tzu-Kang Lin[4] and Nerio Tullini[1]
[1]Department of Engineering, University of Ferrara, Ferrara, Italy
[2]Department of Civil Engineering, National Taiwan University, Taipei, Taiwan
[3]Bridge Engineering Division, National Center for Research on Earthquake Engineering, Taipei, Taiwan
[4]Department of Civil Engineering, National Chiao Tung University, Hsinchu City, Taiwan
*corresponding author: marco.bonopera@unife.it – bonopera@ncree.narl.org.tw

ABSTRACT: This paper compares two nondestructive static methods used for the axial load assessment in prismatic beam–columns of space trusses. Examples include the struts and ties or the tension chords and diagonal braces of steel pipe racks or roof trusses. The first method requires knowledge of the beam–column's flexural rigidity under investigation, whereas the second requires knowledge of the corresponding Euler buckling load. In both procedures, short–term flexural displacements must be measured at given cross sections along the beam–column under examination and subjected to an additional transversal load. The proposed methods were verified by numerical and laboratory tests on beams of a small–scale space truss prototype made from aluminum alloy and rigid connections. In general, if the higher second-order effects are induced during testing and the corresponding total displacements are accurately measured, it would be easy to obtain tensile and compressive force estimations.

Key Words: force identification, inverse problem, second–order theory, space truss, static test

1. INTRODUCTION

Structural safety assessment of beams subjected to axial loads can be required in a space truss to support a restoration project, or to ascertain how close the entire structure is to failure. An accurate evaluation of the *in situ* axial forces is relevant to support the safety analysis of the space truss. In fact, a significant re–distribution of the internal forces can indicate a structural damage or a possible collapse [1]. Forward methods can be used to estimate the axial forces in a beam, e.g. by Finite Element (FE) calculations. Very often, however, an accurate forward estimation of the axial forces can be cumbersome due to uncertainties regarding external loads, support conditions and beam end connections. For this reason, inverse methods have been proposed to evaluate the *in situ* axial forces.

Dynamic methods use vibration responses, measured at several points distributed along the entire structure [2], or a local vibration measurement along the beam–column of interest [3–10]. Most of the existing dynamic methods are based on the identified modal characteristics of a beam–column, i.e. the natural frequencies and/or mode shapes. These modal characteristics depend on the stiffness of the structure and, consequently, are affected by the axial force in the beam. Moreover, the vibration–based estimation of axial loads in space structures requires an accurate selection of the mode shape to be utilized in the identification process. In fact, these methods are particularly sensitive to experimental and model errors. In short, different natural frequencies lead to different accuracies in the axial force estimation. This problem may not be straightforward for a beam of a space truss where global modes may interfere with local modes. Further methods have been proposed to estimate the axial force in a beam–column from the natural frequency of a single mode [11, 12] or multiple modes [13–15]. These methods all rely on the assumption of fixed or hinged end support conditions of the beam. In practice, boundary conditions are often complex and strongly influence the modal characteristics of the structure.

Static methods were originally proposed for the determination of axial forces in a single beam–column [16–19]. Extensions have been made to beam–columns belonging to frame or truss structures [20, 21]. Specifically, Turco [20] proposed a static approach for the axial load identification in bar elements of simple prestressed trusses. Nonetheless, this procedure only considers the bar elements' axial stiffness and, thus, cannot be applied to space trusses because of

the beams' flexural stiffness and rigid or semi–rigid joints. With regards to this feature, Chenaghlou et al. [22] studied a model to predict the moment–rotation behavior of semi–rigid connections in space structures. Instead, Bonopera et al. [21] proposed two static methods for the compressive column load identification in steel space frames using the column's flexural rigidity and a series of horizontal displacements.

In this study, two nondestructive static methods, designed for the axial load estimations in a beam–column, were applied to assess the axial force in space truss members. A comparison of their performance was subsequently obtained.

The first method was based on the procedure proposed by Tullini et al. [16]. This method was successfully applied to tie–rods and simply–supported steel beams in the laboratory but, currently, lacks of experimental simulations on space structures. Specifically, the algorithm can estimate the tensile or compressive force in a beam–column by measuring three displacements along its axis and two displacements in correspondence of the beam ends, subsequent to the application of a transverse load at the midspan. Knowledge of the beam–column's flexural rigidity is required. Nonetheless, a couple applied at the beam ends and the rotational stiffness of the end elastic springs can be unknown.

The second technique is based on the magnification factor method that uses a simplified formula to estimate displacements, taking into account the second–order effects [23, 24]. In particular, the compressive axial load can be identified by measuring one displacement along the member span and two displacements in correspondence of the end constraints when the beam is subjected to an additional lateral load. Knowledge of the Euler buckling load of the beam is also required.

The aforementioned methods use static parameters only and, unlike to dynamic procedures [2–10], do not require selection of the experimental data to be used in the algorithms.

Experimental and numerical tests on a small–scale space truss prototype made from aluminum alloy confirm the robustness of both procedures in presence of moderate measurement errors. Hence, the methods could be profitably applied to beam–columns of large–scale space trusses in the laboratory. *In situ* experiments on steel space trusses are intended in subsequent studies.

2. NONDESTRUCTIVE TESTING (NDT) METHODS

A prismatic beam belonging to a generic plane truss is considered (Fig. 1c). The reference model consists of a beam member of length L constrained by two sets of end elastic springs whose stiffness parameters, depicted for example with $k_{\varphi\varphi}^{(i)}$, $k_{v\varphi}^{(i)}$, $k_{vv}^{(i)}$ (i = 0, 1), are collected by the 2×2 stiffness matrices $\mathbf{K}_0$ and $\mathbf{K}_1$ (Fig. 1a), because the extremities of a truss member can be subjected to displacements and rotations. The beam is subjected to a compressive force N and an additional transverse load F at a generic abscissa $x = a$ (Fig. 1). Elastic modulus E and cross sectional second moment of the area I of each truss member are assumed to be known constants.

The formulations of the two proposed methods are described in the following sections.

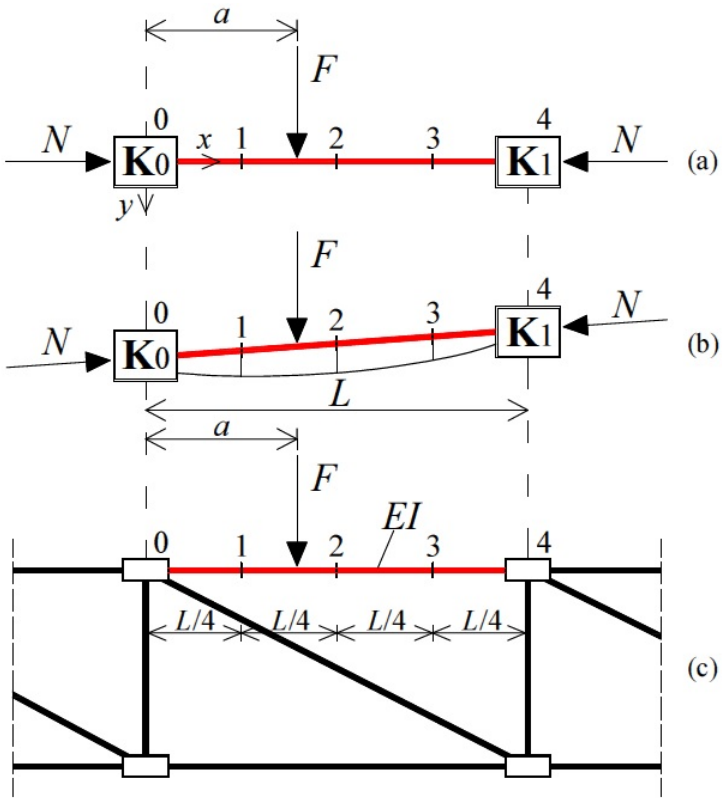

Figure 1. Reference model with location of the instrumented sections (a), deformed shape (b) and prismatic beam under compressive load belonging to a generic truss (c).

2.1. Extension of the method proposed by Tullini et al. [16]

The method proposed by Tullini et al. [16] was extended to generic trusses. This study pointed out that the method lacks of experimental simulations on space structures. Specifically, the algorithm estimates the tensile or compressive load in a beam using three flexural displacements measured along its axis, subsequent to the application of a point load at the midspan. Knowledge of the flexural rigidity EI of the prismatic beam is required. Moreover, a couple applied at the beam ends and the stiffness parameters of the end elastic springs can be unknown (Fig. 1a). To avoid coupling effects of bending and torsion, circular beam cross-section must be considered. With reference to the deformed shape of the beam belonging to the truss in Fig. 1b, the direction of the axial load continues to pass through the beam ends. Therefore, the three displacements v_1, v_2 and v_3 must be referred to the line joining the beam ends (in red), thus requiring the displacement measurements v_0 and v_4 at the end constraints. In fact, the algorithm, when extended to generic trusses, requires the displacement measurements v_1, v_2 and v_3 with respect to the rigid motion of the beam. Thus, the displacements v_1, v_2 and v_3 become respectively equal to $w_1 = (v_1 - 3v_0/4 - v_4/4)$, $w_2 = (v_2 - v_0/2 - v_4/2)$, and $w_3 = (v_3 - v_0/4 - 3v_4/4)$.

Subsequent to the application of point load F at the midspan, i.e., at $x = 2$ in Fig. 1, the five displacements v_0, v_1, v_2, v_3, and v_4 are recorded. By assigning a positive sign to tensile forces, displacements w_1, w_2 and w_3 are used in the following transcendental equation to be solved for the non-dimensional axial load $n = N L^2/EI$:

$$\frac{w_1 + w_3}{w_2} = \frac{1 + 2\cosh(\sqrt{n}/4)}{1 + \cosh(\sqrt{n}/4)} - \frac{\psi}{4w_2} \frac{\sqrt{n}\cosh(\sqrt{n}/4) - 4\sinh(\sqrt{n}/4)}{\sqrt{n^3}\,[1 + \cosh(\sqrt{n}/4)]}, \tag{1}$$

where $\psi = FL^3/EI$ is the load parameter with a length dimension.

In summary, the axial force estimation in a space truss member with unknown couples applied at the beam ends and stiffness parameters of the end elastic springs must conform to the following steps:

1) evaluate the displacements v_0, v_1, v_2, v_3 and v_4 due to a three-point bending test;
2) solve the transcendental Eq. (1) for the unknown constant n using the ratio $(w_1 + w_3)/w_2$ and the expression for ψ;
3) find the analytical value $N_a = n\,EI/L^2$ of the axial force.

2.2. Magnification factor method

In making preliminary design computations of frame or truss structures, it is useful to have an approximate formula for calculating the displacements in beam-columns under compressive axial load. In detail, the total deflection v_{tot}, taking into account the second-order effects, is equal to the product of two terms [23, 24]: the first-order deflection v_I (neglecting the effect of compressive load) and a magnification factor $1/(1 - N/N_{crE})$, where N is the compressive load in the beam-column and N_{crE} is the corresponding first Euler buckling load:

$$v_{tot} = \frac{v_I}{1 - N/N_{crE}}. \tag{2}$$

In general, the simplified formula can be used with good accuracy if the first-order deformed shape of the beam-column and the first Euler buckling shape are similar. Moreover, circular beam cross-section must be considered to avoid coupling effects of bending and torsion.

Equation (2) can be used to estimate the compressive axial force in the beam-column. Subsequent to the application of a point load F, displacements v_0, v_2, and v_4 are recorded (Fig. 1) to compute the total deflection $v_{tot} = (v_2 - v_0/2 - v_4/2)$ at the cross section for $x = 2$. Similarly to the method proposed in [16], the simplified formula (2), when extended to generic trusses, requires the displacement measurement v_2 with respect to the rigid motion of the beam. Then, Eq. (2) can be rearranged to identify the compressive load N as follows:

$$N = N_{crE}\left(1 - \frac{v_I}{v_{tot}}\right). \tag{3}$$

The first-order displacement v_I must be calculated numerically using a FE model of the entire truss, because it is impossible to obtain the *in situ* measurement of deflection v_I owing to second-order effects in the beams of the structure. Similarly, Euler buckling load N_{crE} can be determined numerically using the aforementioned FE model, considering the compressive axial load in the beam-column under investigation in correspondence of the proper Euler buckling load.

In summary, the compressive force identification in a space truss member with unknown couples applied at the beam ends and stiffness parameters of the end elastic springs must conform to the following procedure:

1) in order to compute v_{tot}, measure the displacement v_x at a cross section along the beam span and displacements v_0, v_4 at the beam ends, subsequent to the application of a point load F. Measuring the midspan displacement v_2, i.e., at $x = 2$ in Fig. 1, $v_{tot} = (v_2 - v_0/2 - v_4/2)$;
2) determine numerically, using a FE model, the Euler buckling load N_{crE}, considering the magnitude and position of load F and increasing the carried loads;
3) calculate numerically, using the same FE model, the first-order displacement v_I at the same cross section of displacement v_{tot}, considering the magnitude and position of load F;
4) find the analytical compressive force N_a by Equation (3).

Notably, the load F can be applied at different cross sections along the span, underlining that first-order displacement v_I and experimental displacement v_{tot} must be in reference to the same cross section.

3. APPLICATION OF THE NDT METHODS IN A SPACE TRUSS PROTOTYPE

A space truss prototype with unknown connections was used for the simulations of both NDT methods. The space prototype is a symmetric structure with length of 1800 mm, whereas height and width are 500 and 225 mm, respectively (Fig. 2). It is composed of 80 slender beam-columns made from aluminum alloy and solid circular cross section of 5.0 mm in diameter. The corresponding cross sectional second moment of the area I_{exact} = 30.68 mm^4. All geometric dimensions of the prototype were verified by measuring-systems of 0.01 mm tolerance (laser rangefinder and caliper), once it was fixed on a steel table for laboratory testing (Figs. 3a, b). Yielding stress f_{yk} = 320 MPa and elastic modulus E = 74.13 GPa of the aluminum alloy ("2024–T3" designation) were experimentally evaluated. Specifically, these parameters were identified as mean values from tensile tests on three specimens with solid circular cross sections of 5.0 mm in diameter and 500 mm in length.

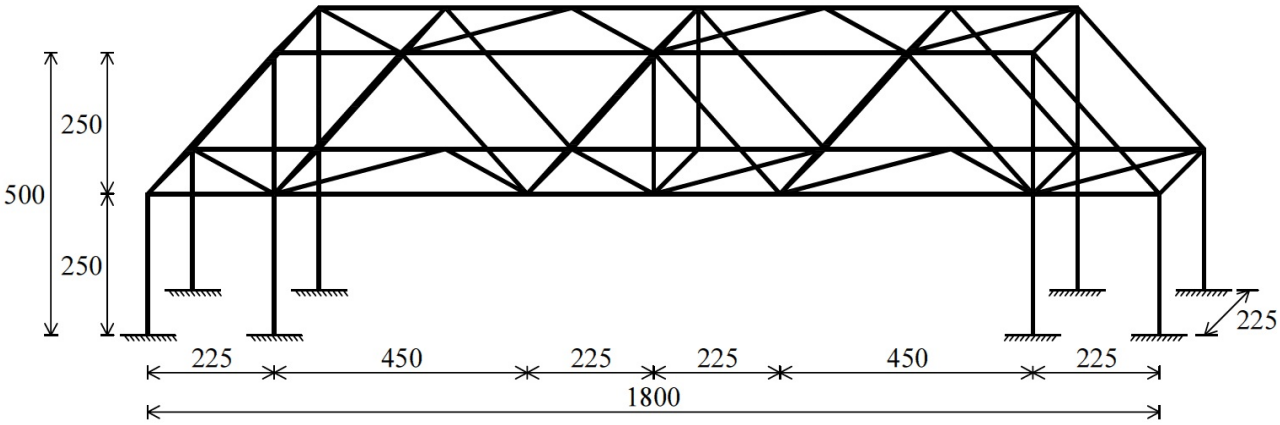

Figure 2. Scheme of the space truss prototype. Units in mm.

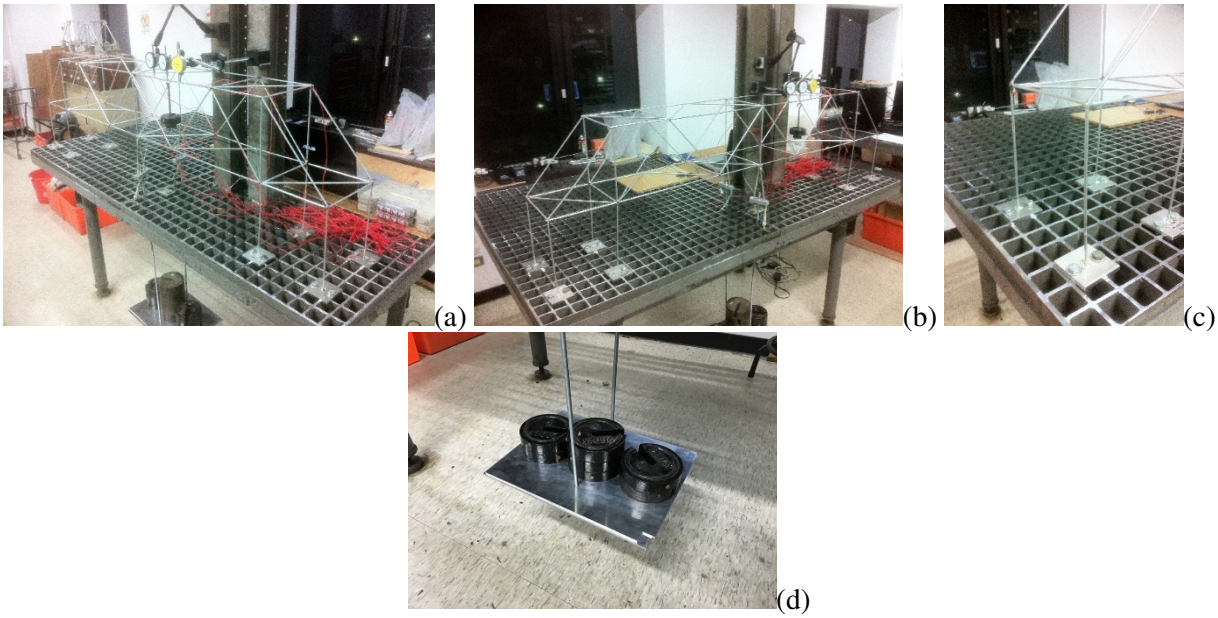

Figure 3. Steel table for the experimental tests (a-b). Fixed restraints and internal rigid joints (c). Vertical point loads P with symmetric layout (d).

The space truss prototype has welded nodes and was fixed on a steel table (Figs. 3a, b), thus bending moments were induced at the boundary conditions and internal joints during static testing. Specifically, vertical point forces P, to simulate the carried loads from real trusses, were applied by adding cast iron disks on a metallic plate positioned at the central part of the prototype in both methods (Figs. 3a, d). Similarly, additional point loads F were assigned by cast iron disks at the midspan of the beams under observation. Pairs of gauges were adhered, diametrically opposite one another, to the beams under investigation where strain was to be measured. Regardless of the axis about which any secondary bending occurs relative to the gauge axis, the axial component of strain

can be taken as the mean of the two measured strains because the equal and opposite bending components cancel out in the averaging, in accordance with Navier's formula of stress distribution. In detail, two pairs of gauges of 5.0 mm in length were longitudinally applied at a distance of 75.0 mm from the beam extremities in accordance with Saint–Venant's principle. Notably, Bahra and Greening used the aforementioned system in the members of a space structure prototype [5, 6]. Additionally, the strain measurements were recorded every second for nearly 40 seconds by a data acquisition unit and during each test combination. The prolonged recording of strains for approximately 40 seconds was caused by a slight oscillation of the strain measurements. The mean value of the strain measurements of the two pairs of gauges was then used to evaluate the existing axial loads N_x. The forces F yielded a variation, ΔN_x, of axial loads N_x owing to the vertical loads P only. The truss prototype was always preserved within the elastic range during the numerical and experimental simulations of both NDT methods.

4. VERIFICATIONS OF THE EXTENSION OF THE METHOD PROPOSED BY TULLINI ET AL. [16]

The experimental and numerical tests used in the extension of the method proposed in [16] are presented. Four values of vertical point force P were applied to the space truss prototype, as reported in Tables 1 and 2. For every assigned load P, a force F was applied at the midspan of two beams subjected to tensile and compressive loads, respectively, then increased progressively up to two different values (Tables 1 and 2). Test combination with P = 48.5 N and F = 21.6 N for the beam subjected to compressive loads was neglected for a temporary lack of accuracy in the strain measurements. Notably, the aforementioned loading condition can be easily viable in laboratory or *in situ* by applying a vertical mass at the midspan of the beam or, eventually, stretching a cable (attached to the beam member) and measuring the force F.

4.1. Experimental tests

4.1.1. Test 1. Beam under tensile axial loads

The test configuration considers the effective beam length $L = L_B$ = 450 mm (Fig. 4). Five short-term displacements v_0, v_1, v_2, v_3, and v_4 of the deflected shape of the beam were measured at equidistant cross sections using dial indicators, after each application of vertical load F (Fig. 5b). Table 1 reports the measured parameters for each combination. The maximum recorded displacement, v_2, was lower than $L_B/60$. Table 1 shows the tensile force evaluations, N_a, obtained by Eq. (1) and the errors $\Delta = [N_a - (N_x + \Delta N_x)]/(N_x + \Delta N_x)$. The comparison between estimated N_a and measured values $N_x + \Delta N_x$ of the tensile loads for each load F is additionally shown in Figures 6a, b, and c. Test 1 provided the better estimations of N_a when the beam was subjected to significant transverse loads F. For instance, the displacement measurements v_1, v_2 and v_3 along the beam axis were greater than 3.50 mm when F = 31.4 N.

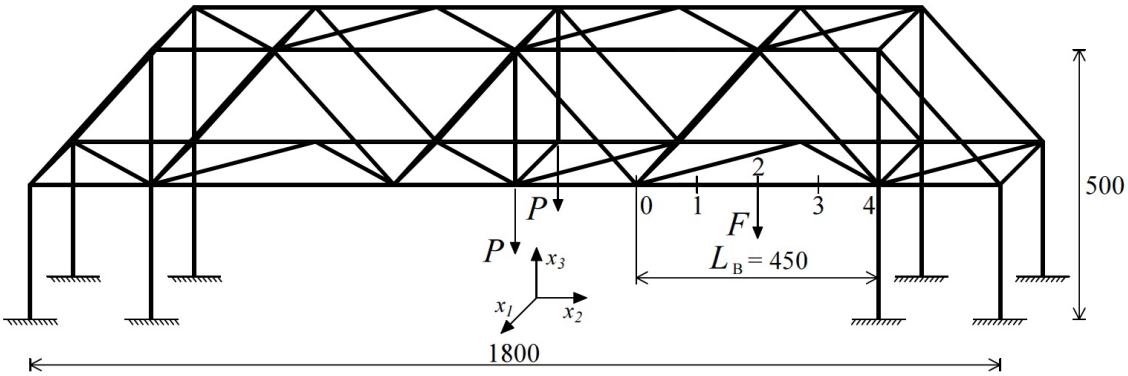

Figure 4. Test 1. Tensile force identifications. Test layout with location of the instrumented sections. Units in mm.


(a)
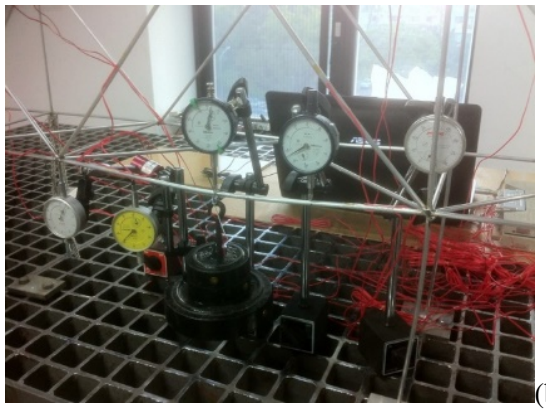
(b)

Figure 5. Test 1. Tensile force identifications. View of experimental tests (a). Deflection of the beam and arrangement of dial indicators and load F (b).

Table 1. Test 1. Tensile force identifications. Measured and estimated parameters

Measured Parameters												Estimated Parameters			
P [N]	N_x [N]	F [N]	$N_x + \Delta N_x$ [N]	v_0 [mm]	v_1 [mm]	v_2 [mm]	v_3 [mm]	v_4 [mm]	w_1 [mm]	w_2 [mm]	w_3 [mm]	ψ [mm]	n	N_a [N]	Δ [%]
68.5	19	21.6	26	0.02	2.86	5.20	2.79	0.03	2.84	5.18	2.76	865	1.4	15	-42.3
133.5	30		39	0.02	2.78	4.99	2.68	0.01	2.76	4.98	2.67	865	3.7	41	5.1
198.5	46		57	0.03	2.62	4.83	2.59	0.01	2.60	4.81	2.58	865	3.9	43	-24.6
238.5	58		66	0.02	2.63	4.73	2.55	0.03	2.61	4.71	2.52	864	5.8	65	-1.5
68.5	19	26.5	31	0.02	3.53	6.34	3.37	0.04	3.51	6.31	3.34	1062	2.0	23	-25.8
133.5	30		42	0.02	3.38	6.08	3.27	0.04	3.36	6.05	3.24	1062	4.1	46	9.5
198.5	46		59	0.04	3.28	5.91	3.19	0.07	3.23	5.86	3.13	1061	4.9	55	-6.8
238.5	58		69	0.04	3.24	5.81	3.14	0.06	3.20	5.76	3.09	1062	6.2	70	1.4
68.5	19	31.4	34	0.04	4.17	7.47	4.01	0.05	4.13	7.43	3.96	1257	2.6	29	-14.7
133.5	30		50	0.09	4.00	7.18	3.87	0.05	3.92	7.11	3.81	1258	4.1	46	-8.0
198.5	46		65	0.04	3.88	6.97	3.75	0.07	3.83	6.92	3.69	1257	5.2	58	-10.8
238.5	58		77	0.10	3.79	6.81	3.70	0.09	3.69	6.72	3.61	1257	6.3	71	-7.8

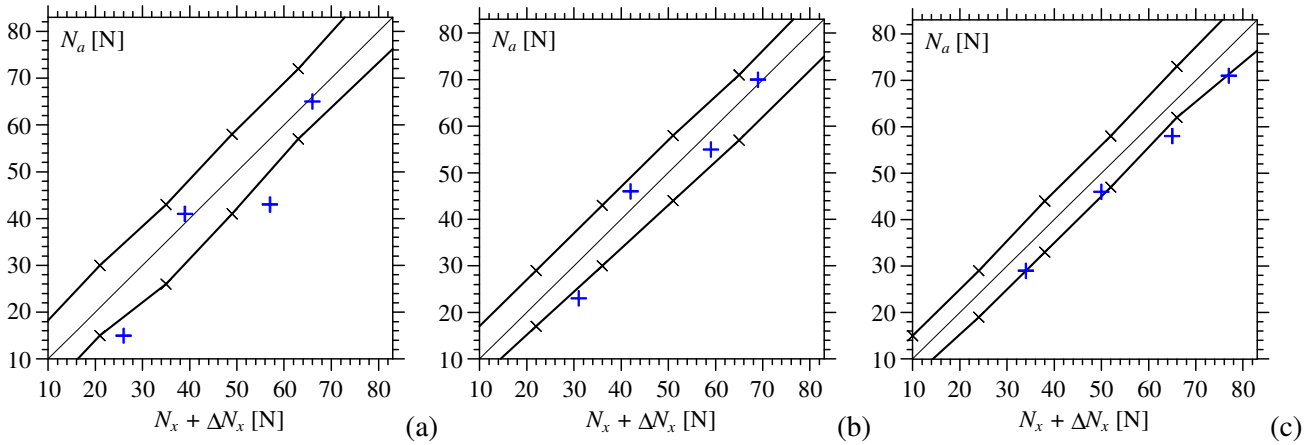

Figure 6. Test 1. Tensile force identifications. Comparison between estimated N_a and measured values $N_x + \Delta N_x$ of the tensile loads when F = 21.6 N (a), 26.5 N (b) and 31.4 N (c). Solid lines with symbol × refer to the sensitivity analyses.

4.1.2. Test 2. Beam under compressive axial loads

The test layout is depicted in Fig. 7. The effective beam length L_B = 450 mm is similarly taken into account. Dial indicators were used to measure the five short-term displacements v_0, v_1, v_2, v_3 and v_4 of the deflected shape of the beam after each application of load F (Figs. 8b, c). Table 2 lists the measured parameters for each test combination. The maximum recorded displacement v_2 was lower than $L_B/55$. The compressive force identifications N_a, evaluated by Eq. (1), are listed in Table 2 with the corresponding errors $\Delta = [N_a - (N_x + \Delta N_x)]/(N_x + \Delta N_x)$. The comparison between estimated N_a and measured values $N_x + \Delta N_x$ of the compressive loads is shown in Figures 9a, b, and c.

Satisfactory estimations of N_a were obtained since all errors Δ were lower than 11%, except for a test case.

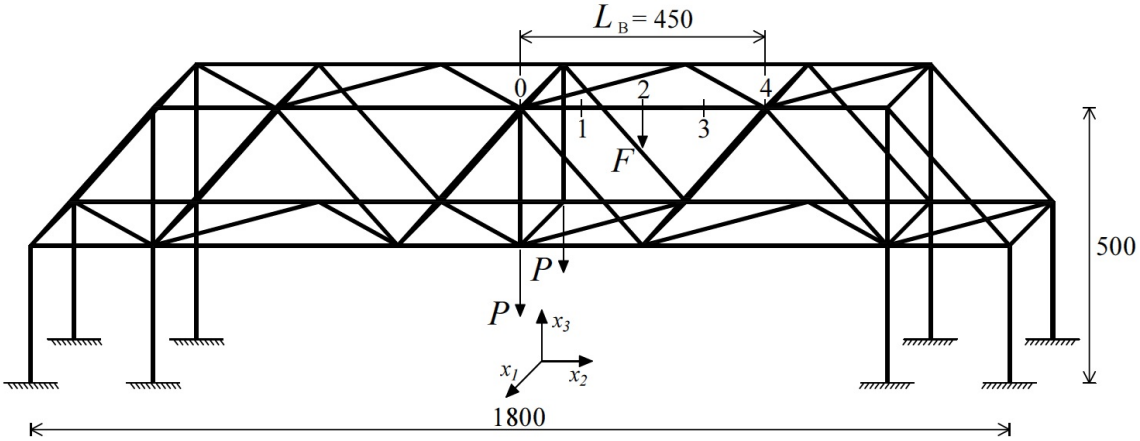

Figure 7. Test 2. Compressive force identifications. Test layout with location of the instrumented sections. Units in mm.

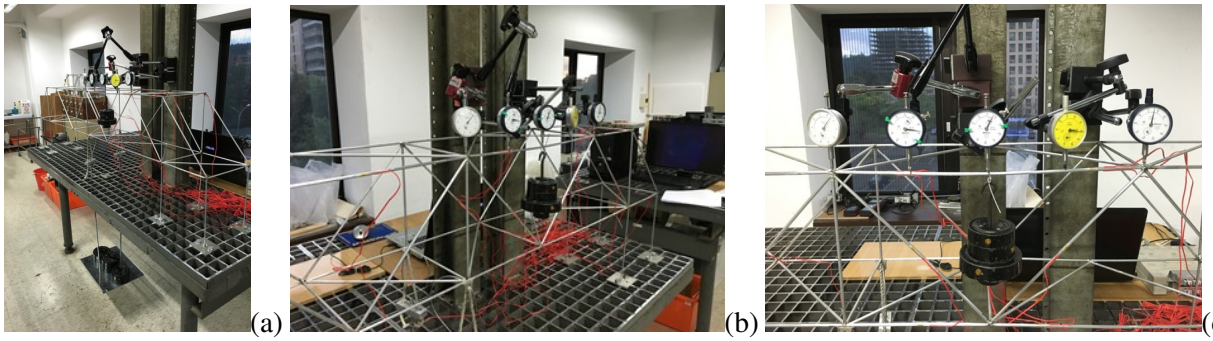

(a) (b) (c)

Figure 8. Test 2. Compressive force identifications. View of experimental tests (a). Deflection of the beam, and arrangement of dial indicators and load F (b-c).

Table 2. Test 2. Compressive force identifications. Measured and estimated parameters

Measured Parameters												Estimated Parameters			
P [N]	N_x [N]	F [N]	$N_x + \Delta N_x$ [N]	v_0 [mm]	v_1 [mm]	v_2 [mm]	v_3 [mm]	v_4 [mm]	w_1 [mm]	w_2 [mm]	w_3 [mm]	ψ [mm]	n	N_a [N]	Δ [%]
48.5	-57	11.8	-63	0.03	1.86	3.47	1.89	0.04	1.83	3.44	1.85	472	-6.1	-68	7.9
		16.7	-71	0.06	2.68	4.96	2.73	0.08	2.62	4.89	2.66	669	-5.4	-61	-14.1
88.5	-71	11.8	-75	0.04	1.99	3.71	2.04	0.06	1.95	3.66	1.99	473	-7.4	-83	10.7
		16.7	-76	0.06	2.87	5.27	2.88	0.09	2.80	5.20	2.80	668	-7.4	-84	10.5
		21.6	-77	0.09	3.75	6.88	3.78	0.11	3.66	6.78	3.68	865	-7.2	-81	5.2
128.5	-104	11.8	-105	0.05	2.23	4.08	2.20	0.07	2.18	4.02	2.14	473	-10.0	-113	7.6
		16.7	-106	0.08	3.16	5.82	3.20	0.08	3.08	5.74	3.12	669	-9.9	-111	4.7
		21.6	-108	0.12	4.18	7.64	4.16	0.09	4.07	7.54	4.06	865	-10.4	-117	8.3
148.5	-114	11.8	-117	0.06	2.37	4.27	2.34	0.07	2.31	4.21	2.27	472	-10.2	-115	-1.7
		16.7	-121	0.08	3.38	6.18	3.34	0.08	3.30	6.10	3.26	669	-11.7	-132	9.1
		21.6	-122	0.14	4.42	8.03	4.39	0.11	4.29	7.91	4.27	865	-11.3	-127	4.1

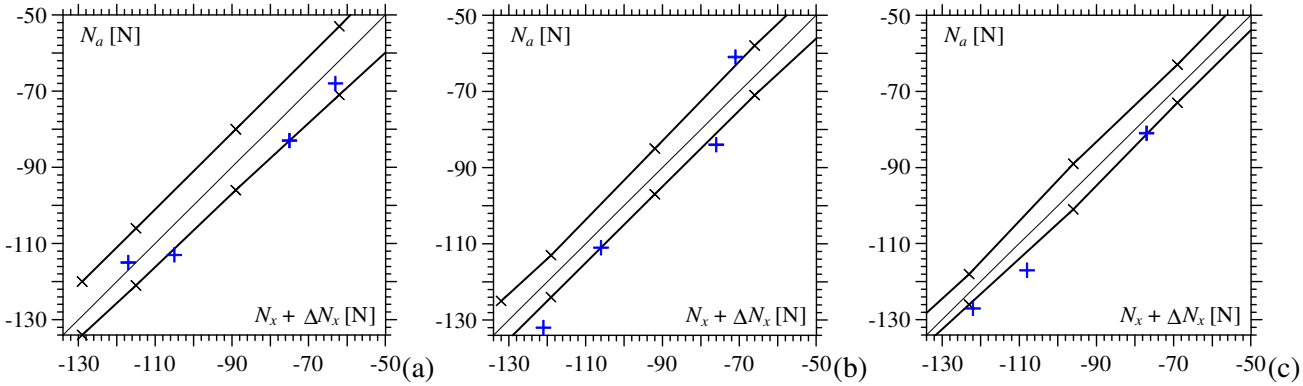

Figure 9. Test 2. Compressive force identifications. Comparison between estimated N_a and measured values $N_x + \Delta N_x$ of the compressive loads when F = 11.8 N (a), 16.7 N (b) and 21.6 N (c). Solid lines with symbol × refer to the sensitivity analyses.

4.2. Analytical verifications

A FE model of the truss prototype was used to determine the five deflections v_0, v_1, v_2, v_3 and v_4 (Fig. 4) using a second-order static analysis without provision for any imperfections in the geometric model. The adopted FE model used four Euler-Bernoulli beam elements for each beam-column. Specifically, the 6 x 6 geometric stiffness matrix of each beam element adopts the exact shape functions described by Bazant and Cedolin [24] in section 2.1. The truss was loaded by two point loads P at the lower nodes of its central part and an additional point load F at the midspan of the beam under investigation, thus simulating Tests 1 and 2. The exact value of the beam's flexural rigidity $EI_{exact} = 74134 \times 30.68 = 2.274 \times 10^6$ N mm^2 was adopted.

To perform a sensitivity analysis for each combination of loads P and F, numerical displacements v_0, v_1, v_2, v_3 and v_4 were alternately modified by adding +0.01 or −0.01 mm to reproduce possible experimental errors. Vice versa, loads F were alternately modified by adding +0.3 or −0.3 N. In total, 16 different combinations of simulated experimental values were obtained.

With reference to Test 1. Table 3 shows the displacements v_0, v_1, v_2, v_3 and v_4 by considering five assigned point loads P when F = 31.4 N located at the midspan. Figures 6a, b, and c show the comparison between worst estimated N_a and assumed values $N_x + \Delta N_x$ in terms of sensitivity analyses when loads F = 21.6, 26.5 and 31.4 N were applied, respectively. A better approximation of the estimated tensile forces was achieved when F = 31.4 N, with the values of N_a lying between $(N_x + \Delta N_x) - 5$ N and $(N_x + \Delta N_x) + 6$ N. Sensitivity analyses (Fig. 6) confirmed that better tensile force estimations can be generally obtained when the beam members are subjected to significant vertical loads, thus increasing the transverse displacements.

With reference to Test 2. Table 4 depicts the displacements v_0, v_1, v_2, v_3 and v_4 for five assigned point loads P when F = 21.6 N at the midspan. Figures 9a, b, and c depict the comparison between worst estimated N_a and assigned values $N_x + \Delta N_x$ in terms of sensitivity analyses when loads F = 11.8, 16.7 and 21.6 N were applied, respectively. Satisfactory approximations of the estimated axial force were obtained when F = 21.6 N. In fact, the values of N_a lie between $(N_x + \Delta N_x) - 4$ N and $(N_x + \Delta N_x) + 6$ N (Fig. 9c). Thus, better identifications of N_a were confirmed when the compression members are subjected to larger lateral loads F and significant second-order effects are induced during testing.

Table 3. Test 1. Tensile force identifications. Displacements computed by the FE model of the truss prototype using EI_{exact} for five values of P and F = 31.4 N

	P [N]	N_x [N]	F [N]	$N_x + \Delta N_x$ [N]	v_0 [mm]	v_1 [mm]	v_2 [mm]	v_3 [mm]	v_4 [mm]
FE model	0	0	31.4	10	0.02	4.33	7.78	4.15	0.01
FE model	67	14	31.4	24	0.02	4.17	7.51	4.02	0.00
FE model	134	28	31.4	38	0.03	4.02	7.27	3.90	0.00
FE model	201	43	31.4	52	0.02	3.90	7.04	3.79	0.00
FE model	268	57	31.4	66	0.03	3.77	6.84	3.69	0.00

Table 4. Test 2. Compressive force identifications. Displacements computed by the FE model of the truss prototype using EI_{exact} for five values of P and F = 21.6 N

	P [N]	N_x [N]	F [N]	$N_x + \Delta N_x$ [N]	v_0 [mm]	v_1 [mm]	v_2 [mm]	v_3 [mm]	v_4 [mm]
FE model	0	0	21.6	-16	0.03	3.13	5.75	3.16	0.02
FE model	40	-26	21.6	-43	0.02	3.39	6.21	3.41	0.02
FE model	80	-53	21.6	-69	0.03	3.68	6.74	3.71	0.02
FE model	120	-79	21.6	-96	0.03	4.05	7.39	4.05	0.02
FE model	160	-106	21.6	-123	0.03	4.50	8.17	4.49	0.02

5. VERIFICATIONS OF THE MAGNIFICATION FACTOR METHOD

The verifications of the magnification factor method are presented in this section. A FE spatial model of the truss is necessary to estimate the Euler buckling load N_{crE} and first-order displacement v_I (Section 2.2).

The displacements v_0, v_2 and v_4, recorded in Test 2 (Table 2), were used to compute the second-order displacements v_{tot}. By contrast, first-order displacements $v_{I,2}$ at the midspan of the beam were calculated using the FE model described in the previous section. In fact, it is not possible to measure the deflections $v_{I,2}$ because the second-order effects, induced by transversal loads P and additional forces F in the beam-columns, cannot be negligible (Figs. 8b, c). The same FE model was used to determine the Euler buckling load, $N_{crE,a3}$ = 399 N, of the beam under investigation. This was done by increasing the two loads P until the global Euler buckling load $P_{crE,a3}$ = 483 N and keeping constant one force $F_{2,x3}$ = 6.9 N at the midspan of the beam, thereby providing a small imperfection in the geometric model. The buckling mode shape of interest is depicted in Figure 10. Notably, a FE buckling analysis provided the correct determination of the Euler buckling load, $N_{crE,a3}$ = 399 N, if the maximum positioning error of force $F_{2,x3}$ is equal to 5.5% of L_B from the midspan of the beam. Figure 11a shows the "load P versus displacement v_{tot}" plot until the buckling load $P_{crE,a3}$ of the space truss was attained.

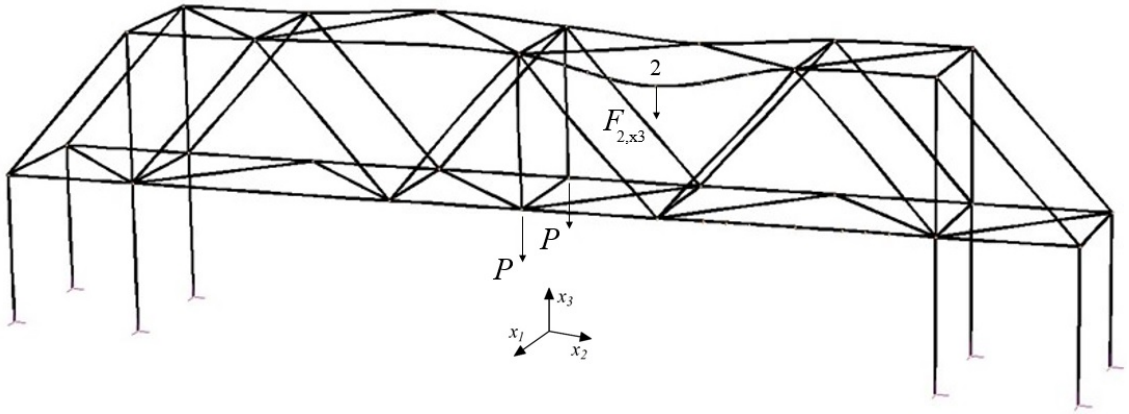

Figure 10. First numerical Euler buckling shape.

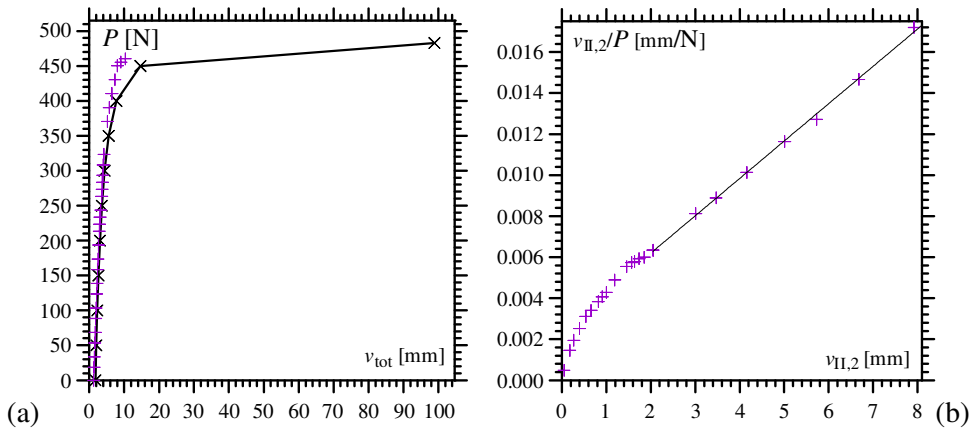

Figure 11. Vertical load P versus displacement v_{tot} plot (a). Southwell plot (b). Symbols + refer to the parameters measured during laboratory tests.

Table 5 reports measured and estimated parameters of the method, where the percentage errors are equal to $\Delta = [N_a - (N_x + \Delta N_x)]/(N_x + \Delta N_x)$. The poor estimates of N_a were given when not significant second-order effects were induced in the tests; in particular, when $N_x + \Delta N_x \leq 71$ N. The identification errors Δ of almost all combinations were lower than 4.0% (in absolute value). Specifically, the minimum compressive load, $N_x + \Delta N_x = 75$ N, corresponding to the range of the satisfactory estimations obtained, was 18.8% of $N_{crE,a3} = 399$ N. Consequently, first-order displacements were magnified by a factor greater than $1/(1 - (N_x + \Delta N_x)/N_{crE,a3}) = 1/(1 - 75/399) = 1/(1 - 0.188) = 1.23$ (Eq. (2)).

Table 5. Compressive force identifications. Measured and estimated parameters

$N_{crE,a3}$ [N]	P [N]	F [N]	$v_{I,2}$ [mm]	$N_x + \Delta N_x$ [N]	v_2 [mm]	N_a [N]	Δ [%]
399	48.5	11.8	3.00	63	3.44	51	-19.0
399	48.5	16.7	4.25	71	4.89	52	-26.8
399	88.5	11.8	3.00	75	3.66	72	-4.0
399	88.5	16.7	4.25	76	5.20	73	-3.9
399	88.5	21.6	5.49	77	6.78	76	-1.3
399	128.5	11.8	3.00	105	4.02	101	-3.8
399	128.5	16.7	4.25	106	5.74	104	-1.9
399	128.5	21.6	5.49	108	7.54	108	0.0
399	148.5	11.8	3.00	117	4.21	115	-1.7
399	148.5	16.7	4.25	121	6.10	121	0.0
399	148.5	21.6	5.49	122	7.91	122	0.0

The evaluation of the global Euler buckling load, $P_{crE,x3}$, was experimentally verified by Southwell's method [25, 26]. A static test was developed by increasing concurrently the loads P and keeping the lateral force $F_{2,x3}$ at the midspan of the beam. The unloaded truss prototype was the reference for the displacement measurements. By using the second-order displacements, $v_{II,2} = v_{tot} - v_{I,2}$, the global Euler buckling load $P_{crE,x3}$ of the truss, with the constant force $F_{2,x3} = 6.9$ N, was estimated as the inverse slope of a Southwell plot, reporting $v_{II,2}/P$ versus $v_{II,2}$ (Fig. 11b). Figure 11a shows the experimental point loads P versus the displacement measurements v_{tot}. Southwell plot is instead depicted in Figure 11b. The least squares method was then used to estimate the inverse slope, leading to $P_{crE,x3} = 549$ N. The global buckling load $P_{crE,x3}$ was 13.7% greater than the analytical one $P_{crE,a3}$ equal to 483 N and showed in Figure 11a. Euler buckling load $N_{crE,x3} = 368$ N was then obtained using the corresponding axial force in the beam (under observation) belonging to the FE model and assigning the loading arrangement $P_{crE,x3} + P_{crE,x3}$ and $F_{2,x3}$. Any geometric imperfection was induced in the FE model. Thus, the experimental value $N_{crE,x3}$ was of 7.8% lower than the analytical one $N_{crE,a3}$.

6. CONCLUSIONS

This paper reports two nondestructive static methods for the assessment of axial loads in generic space trusses. Both procedures use bending tests and corresponding measured displacements along the member under investigation, subsequent to the application of an additional point load. Experiments on a small-scale space truss prototype confirmed that tensile and compressive force identifications through the method proposed by Tullini et al. [16] are feasible even with uncertain rotational boundary conditions. The accuracy of tensile force estimations improves by increasing the point load, thus inducing displacements greater than 3.50 mm. Vice versa, a magnification factor greater than 1.45 is required to obtain better compressive force identifications. Sensitivity analyses confirmed that satisfactory estimations can be generally obtained if the test measurements

are accurately recorded. The magnification factor method, based on a simplified formula [23, 24], similarly requires significant second-order effects induced in the truss member during testing. An identification error lower than 10% can be obtained when the magnification factor is greater than 1.23. To preserve the truss members within the elastic range, a preliminary calculation of the required additional load must be performed for both methods, based on the geometrical and mechanical properties of the truss to investigate. The proposed methods could be applied *in situ* after further studies and simulations on real trusses using the high potential of Fiber Bragg grating-differential settlement measurement (FBG-DSM) sensors for the short-term recording of the displacements [18, 27–30]. Safety inspections will increasingly become important in the near future, especially because of the improvement of material properties that will allow to design space trusses composed of highly slender members. Finally, Southwell's method confirmed the evaluation of the Euler buckling load conducted using a FE model of the space truss prototype.

ACKNOWLEDGMENTS

M.B. acknowledged the financial support of the "Tender for Young Researchers Abroad Grant" in 2014 provided by the University of Ferrara, Italy, and the "Summer Program in Taiwan Grant" in 2014 and 2015 provided by the Ministry of Science and Technology of Taiwan for European Ph.D. candidates. N.T. acknowledged the financial support of the "Research Program FAR 2018" provided by the University of Ferrara. The experiments were supported by funding from the National Applied Research Laboratories Project of Taiwan (NCREE-06104A1700). Finally, special gratitude is extended to the technicians and students of National Taiwan University, who provided considerable assistance to the authors.

CONFLICT OF INTEREST

The authors declare no conflict of interest with respect to the research, authorship and publication of this article.

REFERENCES

1. Hui-Jun L, Zeng-Li P, Chun-Liang Y, et al. Application of advanced reliability algorithms in truss structures. *Int J Space Struct* 2014; 29 :61–70.
2. Greening P and Lieven N. Identification and updating of loading in frameworks using dynamic measurements. *J Sound Vib* 2003; 260 :101–115.
3. Park S, Choi S, Oh S, et al. Identification of the tensile force in high-tension bars using modal sensitivities. *Int J Solids Struct* 2006; 43 :3185–3196.
4. Tullini N and Laudiero F. Dynamic identification of beam axial loads using one flexural mode shape. *J Sound Vib* 2008; 318 :131–147.
5. Bahra AS and Greening PD. Identifying axial load patterns using space frame FEMs and measured vibration data. *Mech Syst Signal Process* 2009; 23 :1282–1297.
6. Bahra AS and Greening PD. Identifying multiple axial load patterns using measured vibration data. *J Sound Vib* 2011; 330 :3591–3605.
7. Rebecchi G, Tullini N and Laudiero F. Estimate of the axial force in slender beams with unknown boundary conditions using one flexural mode shape. *J Sound Vib* 2013; 332 :4122–4135.
8. Maes K, Peeters J, Reynders E, et al. Identification of axial forces in beam members by local vibration measurements. *J Sound Vib* 2013; 332 :5417–5432.
9. Luong HTM, Zabel V, Lorenz W, et al. Vibration-based model updating and identification of multiple axial forces in truss structures. *Procedia Eng* 2017a; 188 :385–392.
10. Luong HTM, Zabel V, Lorenz W, et al. Non-destructive assessment of the axial stress state in iron and steel truss structures by dynamic measurements. *Procedia Eng* 2017b; 199 :3380–3385.
11. Zui H, Shinke T and Namita Y. Practical formulas for estimation of cable tension by vibration method. *J Struct Eng* 1996; 122 :651–656.

12. Mehrabi A and Tabatabai H. Unified finite difference formulation for free vibration of cables. *J Struct Eng* 1998; 124 :1313–1322.
13. Geier R, De Roeck G and Flesch R. Accurate cable force determination using ambient vibration measurements. *Struct Infrastruct Eng* 2006; 2 :43–52.
14. Lagomarsino S and Calderini C. The dynamical identification of the tensile force in ancient tie-rods. *Eng Struct* 2005; 27 :846–856.
15. Amabili M, Carra S, Collini L, et al. Estimation of tensile force in tie-rods using a frequency-based identification method. *J Sound Vib* 2010; 329 :2057–2067.
16. Tullini N, Rebecchi G and Laudiero F. Bending tests to estimate the axial force in tie-rods. *Mech Res Commun* 2012; 44 :57–64.
17. Tullini N. Bending tests to estimate the axial force in slender beams with unknown boundary conditions. *Mech Res Commun* 2013; 53 :15–23.
18. Bonopera M, Chang KC, Chen CC, et al. Axial load detection in compressed steel beams using FBG–DSM sensors. *Smart Struct Syst* 2018a; 21 (1) :53–64.
19. Bonopera M, Chang KC, Chen CC, et al. Feasibility study of prestress load prediction in concrete beams using second–order deflections. *Int J Struct Stab Dy* 2018b.
20. Turco E. Identification of axial forces on statically indeterminate pin-jointed trusses by a nondestructive mechanical test. *Open Civil Eng J* 2013; 7 :50–57.
21. Bonopera M, Chang KC, Chen CC, et al. Compressive column load identification in steel space frames using second–order deflection–based methods. *Int J Struct Stab Dy* 2018c; 18 (7) art. ID 1850092.
22. Chenaghlou MR, Nooshin H and Harding JE. Proposed mathematical model for semi-rigid joint behaviour (M-θ) in space structures. *Int J Space Struct* 2014; 29 :71–80.
23. Timoshenko SP and Gere JM. *Theory of Elastic Stability*. McGraw-Hill, New York, 1961.
24. Bazant ZP and Cedolin L. *Stability of Structures*. Oxford University Press, New York, 1991.
25. Southwell RV. *On the analysis of experimental observations in problems of elastic stability*. Proceedings Royal Society London series A, 1932, 601–616.
26. Singer J, Arbocz J and Weller T. *Buckling experiments: experimental methods in buckling of thin-walled structures: basic concepts, columns, beams and plates*. Vol. 1, John Wiley & Sons, Inc, 1998.
27. Chang KC, Lee ZK and Chen CC. Structural assessment of a repaired cable bridge damaged in 1999 Chi-Chi earthquake. In: *International Symposium on Engineering Lessons Learned from the 2011 Great East Japan Earthquake*, March 1–4 2012, Tokyo, Japan.
28. Lee ZK. *Bridge safety monitoring integrated system with full optical fiber and the method for sensing thereof*. Patent No. 5542980, Japan, 2014.
29. Lee ZK. *Bridge safety monitoring integrated system with full optical fiber and the method for sensing thereof*. Patent No. 9183739, USA, 2015.
30. Lai CC, Au HY, Liu MSY, et al. Development of level sensors based on fiber Bragg grating for railway track differential settlement measurement. *IEEE Sens J* 2016; 16 :6346–6350.